Compound I and Compound II Analogues from Porpholactones

K. Jayaraj, A. Gold,* R. N. Austin,† and L. M. Ball

Department of Environmental Sciences and Engineering, University of North Carolina at Chapel Hill, Chapel Hill, North Carolina 27599-7400

J. Terner*

Department of Chemistry, Virginia Commonwealth University, Richmond, Virginia 23284-2006

D. Mandon, R. Weiss,* J. Fischer, and A. DeCian

Institut LeBel, Université Louis Pasteur, 67070 Strasbourg, France

E. Bill

Max-Planck-Institut für Strahlenchemie, 45470 Mülheim/Ruhr, Germany

M. Müther, V. Schünemann, and A. X. Trautwein*

Institut für Physik, Medizinische Universität zu Lübeck, D-23538 Lübeck, Germany

Received May 19, 1997[⊗]

The tetraaza macrocycles 2-oxa-3-oxotetramesitylporphine (|H_2 **1**|) and 2-oxa-3-oxotetrakis(2,6-dichlorophenyl)-porphine (|H_2 **2**|) and the corresponding iron complexes (|Fe^{III}(X) **1**| and |Fe^{III}(X) **2**|; X= Cl^-, OH^-, or $SO_3CF_3^-$) have been synthesized. These macrocycles are derived from porphyrins by transformation of one pyrrole ring to an oxazolone ring. The resulting lactone functionality serves to restrict but not completely block π-conjugation around the periphery. These complexes thus share properties with both porphyrins and chlorins. The ferric and high-valent iron complexes have been characterized by a variety of spectroscopic techniques. The molecular structure of |Fe^{III}(Cl) **2**| has been obtained by X-ray crystallography and shows that the structural changes at the macrocycle periphery do not perturb the coordination sphere of iron relative to the corresponding porphyrin complexes. This is illustrated by the observation that Fe−O frequencies in the resonance Raman spectra of the porpholactone analogues of compounds I and II are not substantially different from those of porphyrins and by the axial appearance of the EPR signals of the high-spin ferric complexes. This is consistent with reports that the Fe=O unit of oxidized porphyrins and chlorins is relatively insensitive to alteration of macrocycle symmetry. Nevertheless, probes of properties of the porpholactone macrocycle (^{1}H NMR, resonance Raman skeletal modes) show effects of the asymmetry induced by the oxazolone ring. On the basis of ^{1}H NMR, EPR, Mössbauer, and resonance Raman data, the singly occupied molecular orbital of oxoferryl porpholactone π-cation radicals correlates with the a_{1u} molecular orbital of porphyrins under D_{4h} symmetry. Moreover, the paramagnetic properties and the intramolecular exchange interaction of ferryl iron and the porpholactone π-radical have been characterized by EPR and magnetic Mössbauer measurements and spin-Hamiltonian analyses. The values $J_0 = 17$ cm^{-1} and $J_0 = 11$ cm^{-1} obtained for the exchange coupling constants of the oxoferryl porpholactone π-cation radical complexes |Fe^{IV}=O **1**|$^+$ and |Fe^{IV}=O **2**|$^+$, respectively, are among the lowest found for synthetic compound I analogues.

Introduction

The oxoferryl porphyrin π-cation radical (compound I) and oxoferryl porphyrin (compound II) transients are key intermediates in the catalytic cycles of peroxidases[1] catalases,[2] and oxidases.[3] Recently, the identification of chlorins as prosthetic groups of peroxidases,[4] catalases[5−7] and oxidases[8−12] has stimulated interest in high-valent iron complexes of partially saturated porphyrins having electronic structures congruent with those of compound I and compound II. The porpholactone

† Current address: Bates College, Department of Chemistry, Lewiston, ME 04240.

⊗ Abstract published in *Advance ACS Abstracts,* August 15, 1997.

(1) Marnett, L. J.; Kennedy, T. A. in *Cytochrome P450: Structure, Mechanism, and Biochemistry,* 2nd ed.; Ortiz de Montellano, P. R., Ed.; Plenum Press: New York, 1995; pp 49−83.
(2) Hewson, W. D.; Hager, L. P. In *The Porphyrins, Part VII*; Dolphin, D., Ed.; Academic Press: New York, 1978; pp 295−332.
(3) Ogura, T.; Hirota, S.; Proshlyakov, D. A.; Shinzawa-Itoh, K.; Yoshikawa, S.; Kitagawa, T. *J. Am. Chem. Soc.* **1996**, *118*, 5443−5449.
(4) Patterson, W. R.; Poulos, T. L.; Goodin, D. B. *Biochemistry* **1995**, *34*, 4342−4345.
(5) Jacob, G. S.; Orme-Johnson, W. H. *Biochemistry* **1979**, *18*, 2975−2980.
(6) Chiu, J. T.; Loewen, P. C.; Switala, J.; Gennis, R. B.; Timkovich, R. *J. Am. Chem. Soc.* **1989**, *111*, 7046−7050.
(7) Benecky, M. J.; Frew, J. E.; Scowen, N.; Jones, P.; Hoffman, B. M. *Biochemistry* **1993**, *32*, 11929−11933.
(8) Timkovich, R.; Bondoc, L. L. *Adv. Biophys. Chem.* **1990**, *1*, 203−247.
(9) Vavra, M. R.; Timkovich, R.; Yap, F.; Gennis, R. B. *Arch. Biochem. Biophys.* **1986**, *250*, 461−468.

S0020-1669(97)00597-1 CCC: $14.00

structure is formally derived by transformation of one pyrrole ring of a porphyrin macrocycle to an oxazolone ring.[13] Because the lactone function participates to some extent in the macrocycle π-system,[13] porpholactones are intermediate to porphyrins and chlorins. Characterization of oxoferryl porpholactone π-cation radical systems can be expected to provide insights into effects of partial macrocycle saturation on symmetry state and exchange coupling between the unpaired electron spins of ferryl iron and the ligand π-cation radical in compound I analogues. This report describes the synthesis of porpholactones 2-oxa-3-oxotetramesitylporphine ($|H_2$ **1**$|$) and 2-oxa-3-oxotetrakis(2,6-dichlorophenyl)porphine ($|H_2$ **2**$|$), metalation to the corresponding iron complexes ($|Fe^{III}(X)$ **1**$|$ and $|Fe^{III}(X)$ **2**$|$; X = monovalent anion), and the molecular structure of $|Fe^{III}(Cl)$ **2**$|$ by X-ray crystallography. High-valent iron complexes of the porpholactones are generated and compared to those of the analogous porphyrins.

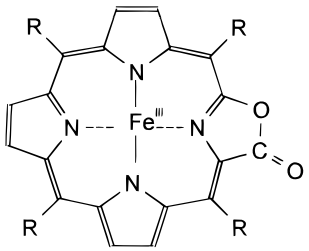

R= 2,4,6-trimethylphenyl or 2,6-dichlorophenyl

Experimental Section

General Methods. Solvents were dried and distilled before use. Commercial (Aldrich) *m*-chloroperoxybenzoic acid (*m*-CPBA) was dried by being dissolved in methylene chloride and treated with magnesium sulfate.

Variable temperature UV−vis spectra were recorded on a Varian Cary 05E spectrometer equipped with an Oxford Instruments liquid nitrogen cryostat, DN1704. Reactions were performed directly in the spectrometer beam in an optical quartz reaction vessel sealed to a Schlenk head. Cyclic voltammetry was performed on an EG&G Princeton Applied Reaearch potentiostat/galvanostat, Model 273A, with working and auxiliary platinum electrodes and using the saturated calomel electrode as the reference. The supporting electrolyte was $TBAPF_6$, 0.1 M in CH_2Cl_2, and the scan rate was 200 m Vs^{-1}. ^1H NMR spectra were recorded on a Bruker AMX spectrometer, and chemical shifts are given in ppm relative to TMS. Mass spectra were obtained on a VG 70-250 SEQ mass spectrometer operating in the FAB mode, with a *p*-nitrobenzyl alcohol matrix. Resonance Raman signals were detected by an optical multichannel analyzer (EG&G Princeton Applied Research Corp., Model 1460) with a Model 1420 intensified reticon detector head. The excitation source was a krypton ion laser (Spectra-Physics Model 171) equipped with an ultrahigh-field magnet. The sample was contained in a spinning quartz cell that was maintained at −80 °C in a thermostated quartz enclosure with cold N_2 gas. Scattered light was collected at 90° through an optically clear wall of the enclosure by a 50 mm *f*/0.95 Canon lens and imaged by a quartz 180 mm *f*/4.5 lens (Melles Griot) onto the slit of a Spex Model 1870 0.5 m spectrograph. EPR spectra were recorded on a Bruker ER200D-SRC spectrometer equipped with an Oxford Instruments liquid-helium cryostat, Model ESR 910. Temperature measurements were calibrated using Curie−Weiss behavior of the signal of a ferric low-spin standard (ferric cytochrome *c*). Temperature stability was on the order of 0.2 K, and from measurements with a carbon glass resistor, the temperature gradient across the sample was found to be less than 0.5 K. The Mössbauer spectra were recorded using a conventional spectrometer in the constant-acceleration mode. The spectra obtained at low fields (20 mT) were measured in a He bath cryostat (Oxford Instruments, MD 306) equipped with a pair of circular permanent magnets. For the high-field spectra a cryostat with a superconducting magnet was used (Oxford Instruments). Isomer shifts are given relative to metallic iron (α-Fe) at room temperature.

Spin Hamiltonian Simulations. EPR spectra of the oxoferryl porphyrin π-radical complex were simulated using the spin Hamiltonian

$$H_e = D[S_z^2 - 2/3 + E/D(S_x^2 - S_y^2)] + \mu_B(\mathbf{S}\cdot\mathbf{g} + g'\mathbf{S}')\cdot\mathbf{B} - \mathbf{S}\cdot\mathbf{J}\cdot\mathbf{S}' \quad (1)$$

which includes zero-field splitting (ZFS), electronic Zeeman interaction, and exchange in the intrinsic spin representation of the coupled $S = 1$ (Fe(IV)═O) and $S' = {}^1/_2$ (π-radical) systems. The electronic coupling tensor $\mathbf{J} = \mathbf{1}J_0 + \mathbf{J}^a$ consists of an isotropic part J_0 and a traceless anisotropic tensor $\mathbf{J}^a$. The components of $\mathbf{J}^a$ were constrained to values consistent with recent theoretical considerations.[14] The local **g** tensor of ferryl iron was correlated to the zero-field splitting parameters *D* and *E/D* using an extended ligand-field model[15] with the one-electron spin−orbit coupling constant ζ taken[16] as 500 cm^{-1}. It was shown recently for the case of $TMP(Fe^{IV}{=}O)^+$ that the latter procedure leads to an overestimation[14] of the local $g_{x,y}$ values of the ferryl ion by about 5%. A corresponding readjustment of the local *g* values leads to no significant improvement of the simulations presented below. For the radical spin, g' was fixed at 2.0. The EPR spectra were simulated with eq 1 using a "*g*-strain" model for the line shape,[17] which is based on a Gaussian distribution of spin-Hamiltonian parameters leading to an angular variation of Gaussian line widths.

EPR spectra of the ferric starting material decomposition products and Fe(III) low-spin species were simulated using effective g values and Gaussian line shapes with angular dependence. Spin quantitations were performed by double integration of simulated absorption-derivative subspectra and comparison with the ferric starting material; differences in *g* values were taken into account by using the Aasa *g* factors[18] for corrections.

Magnetic Mössbauer spectra were simulated using eq 1 together with the usual nuclear Hamiltonian H_N:[19]

$$H = H_e + H_N \quad (2)$$

$$H_N = eQV_{zz}(4I(I+1))^{-1}[3I_z^2 - I(I+1) + \eta(I_x^2 - I_y^2)] - g_N\mu_N\mathbf{I}\cdot\mathbf{B} + \langle\mathbf{S}\rangle\cdot\mathbf{A}\cdot\mathbf{I} \quad (3)$$

Within H_N, *I* denotes the nuclear spin, *Q* the nuclear quadrupole moment of the excited nuclear state of ^{57}Fe, V_{zz} the main component of the electric-field gradient tensor, and $\eta = (V_{xx} - V_{yy})/V_{zz}$ is the asymmetry parameter of the electric-field gradient. **A** denotes the hyperfine coupling tensor, g_N the nuclear *g* factor, and μ_N the nuclear magneton.

2-Nitrotetramesitylporphine.[20] To zinc(II) tetramesitylporphyrin[21,22] (509 mg) in methylene chloride (100 mL) and acetonitrile (70 mL) was added $AgNO_2$ (122 mg) in acetonitrile (5 mL) followed by iodine (100 mg) in dichloromethane (45 mL). The mixture

(10) Kahlow, M. A.; Zuberi, T. M.; Gennis, R. B.; Loehr. T. M. *Biochemistry* **1991**, *30*, 11485−11489.
(11) Timkovich, R.; Cork, M. S.; Gennis, R. B.; Johnson, P. Y. *J. Am. Chem. Soc.* **1985**, *107*, 6069−6075.
(12) Jiang, F. S.; Zuberi, T. M.; Cornelius, J. B.; Clarkson, R. B.; Gennis, R. B.; Belford, R. L. *J. Am. Chem. Soc.* **1993**, *115*, 10293−10299.
(13) Gouterman, M.; Hall, R. J.; Gamal-Eddin, K.; Martin, P. C.; Shankland, E. G.; Cerney, R. L. *J. Am. Chem. Soc.* **1989**, *111*, 3702−3707.
(14) Paulsen, H.; Müther, M.; Grodzicki, M.; Trautwein, A. X.; Bill, E. *Bull. Soc. Chim. Fr.* **1996**, *133*, 703−710.
(15) Oosterhuis, W. T.; Lang, G. *J. Chem. Phys.* **1973**, *58*, 4757−4765.
(16) Mandon, D.; Weiss, R.; Jayaraj, K.; Gold, A.; Terner, J.; Bill, E.; Trautwein, A. X. *Inorg. Chem*. **1992**, *31*, 4404−4409.
(17) Schulz, C. E.; Rutter, R.; Sage, J. T.; Debrunner, P. G.; Hager, L. P. *Biochemistry* **1984**, *23*, 4743−4754.
(18) Aasa, R.; Vånngard, T. *J. Magn. Reson.* **1975**, *19*, 308−315.
(19) Trautwein, A. X.; Bill, E.; Bominaar, E. L.; Winkler, H. *Struct. Bonding* **1991**, *78*, 1−95.
(20) Catalano, M. M.; Crossley, M. J.; Harding, M. M.; King, L. G. *J. Chem. Soc., Chem. Commun.* **1984**, 1535−1538.
(21) Lindsey, J. S. D.; Schreiman, I. G.; Hsu, H. C.; Kearney, P. C.; Marguerettaz, A. M. *J. Org. Chem.* **1987**, *52*, 827−836.
(22) Adler, A. D.; Longo, F. R.; Kampas, F.; Kim, J. J. *Inorg. Nucl. Chem.* **1970**, *32*, 2443−2445.

was stirred at room temperature in the dark for 0.5 h, after which the solvent was evaporated and the Zn complex obtained by chromatography of the residue on silica eluted with 1:1 hexane/methylene chloride (second band off the column). Treatment of the Zn complex with 5% trifluoroacetic acid/methylene chloride gave the metal-free base (397 mg; 78%). ^{1}H NMR (500 MHz, chloroform-*d*): 8.85 (s, 1H, py-H3), 8.80 (d, 1 H, py-H, $J = 4.4$ Hz), 8.77 (d, 1 H, py-H, $J = 4.4$ Hz), 8.73 (d, 1 H, py-H, $J = 5.4$ Hz), 8.72 (d, 1 H, py-H, $J = 5.4$ Hz), 8.59 (s, 2 H, py-H), 7.26 (bs, 4H, mesityl *m*-H), 7.26 (bs, 2 H, mesityl *m*-H), 7.16 (bs, 2 H, mesityl *m*-H), 2.6 (m, 12H, mesityl *p*-CH_3), 1.9 (m, 24H, mesityl *o*-CH_3), −2.5 (s, 2H, N*H*) ppm. FAB MS (*p*-nitrophenol matrix): MH$^+$, *m/z* 828.

2-Oxa-3-oxotetramesitylporphine[23] **(|H$_2$ 1|).** To a mixture of 2-nitrotetramesitylporphine (203 mg) and 10% Pd/C (202 mg) in 1:1 anhydrous methanol/methylene chloride (200 mL) under Ar was added $NaBH_4$ (450 mg) in one portion, and the reaction mixture was stirred for 2.5 h. A second portion of $NaBH_4$ (80 mg) was added and stirring continued for 0.5 h. Following filtration and evaporation of the solvent, the crude product mixture was stirred in methylene chloride (200 mL) with *m*-CPBA (220 mg) for 2 h. |H$_2$ **1**| was isolated by chromatography on silica eluted with 1:1 hexane/methylene chloride (150 mg; 72%). ^{1}H NMR (500 MHz, chloroform-*d*): 8.5 (m, 6H, py-H), 7.3 (d, 8H, mesityl *m*-H), 2.6 (m, 12H, mesityl *p*-CH_3), 1.8 (m, 24H, mesityl *o*-CH_3), −1.5 (s, 1H, N*H*), −1.9 (s, 1H, N*H*) ppm. FAB MS (*p*-nitrophenol matrix): MH$^+$, *m/z* 801.

Chloro(2-oxa-3-oxotetramesitylporphinato)iron(III) |Fe^{III}(Cl) 1|. The ferric complex was obtained quantitatively by refluxing the metal-free base with ferrous chloride ($^{57}FeCl_2$ for Mössbauer spectroscopy)[16,22] in dimethylformamide (DMF). ^{1}H NMR (500 MHz, chloroform-*d*): 88.3, 83.8, 83.2, 82.0, 75.2, 72.2 (bs, 1:1:1:1:1:1 H, py-H), 17.4, 17.2, 15.7, 15.3, 15.2, 13.6. 13.5 (s, 1:1:2:1:1:1:1 H, mesityl *m*-H), 7.8, 6.5 (v bs, 1:3 H, mesityl *o*-CH_3) ppm. HRMS (FAB): calcd for $C_{55}H_{50}N_4O_2Fe$ 854.3241, found 854.3283. Anal. Calcd for $C_{55}H_{50}N_4O_2FeCl{\cdot}CH_3OH$: C, 72.96; H, 5.90; N, 6.10; Fe, 6.05. Found: C, 73.06; H, 6.36; N, 6.09; Fe, 5.68.

2-Nitrotetrakis(2,6-dichlorophenyl)porphine. The procedure described above for preparation of 2-nitrotetramesitylporphine gave 2-nitrotetrakis(2,6-dichlorophenyl)porphine in 44% yield. ^{1}H NMR (500 MHz, methylene-d_2 chloride): 8.93 (s, 1 H, py-H3), 8.84 (d, 1 H, py-H, $J = 5.1$ Hz), 8.81 (d, 1 H, py-H, $J = 5.1$ Hz), 8.78 (bs, 1 H, py-H), 8.61 (d, 1 H, py-H, $J = 4.5$ Hz), 8.59 (d, 1 H, py-H, $J = 4.5$ Hz), 7.9−7.7 (m, 12 H, phenyl *m*-, *p*-H), −2.5 (s, 1 H, N*H*) ppm. FAB MS (*p*-nitrobenzyl alcohol matrix): M$^+$, cluster at *m/z* 935, pattern consistent with eight Cl atoms.

2-Oxa-3-oxotetrakis(2,6-dichlorophenyl)porphine. To 2-nitrotetrakis(2,6-dichlorophenyl)porphine (173 mg) and 10% Pd/C (164 mg) in 1:1 anhydrous methanol/methylene chloride (160 mL) under Ar was added $NaBH_4$ (600 mg) over 20 min. After stirring for 3 h, the Pd/C was removed by filtration, the solvent evaporated under reduced pressure, and the residue stirred with *m*-CPBA (355 mg) in 1:1 methylene chloride/chloroform for 16 h. The product was purified by chromatography on silica eluted with 1:1 hexane/methylene chloride, yielding 72 mg (42%). ^{1}H NMR (500 MHz, chloroform-*d*): 8.7 (m, 1 H, py-H), 8.6 (m, 2 H, py-H), 8.5 (m, 1 H, py-H), 8.4 (d, 1 H, py-H), 8.3 (d, 1 H, py-H), 7.7 (m, 12 H, phenyl *m*-, *p*-H), −1.5 (s, 1 H, *N*H), −1.9 (s, 1 H, *N*H) ppm. FAB MS (*p*-nitrobenzyl alcohol matrix): M$^+$, cluster at *m/z* 908, consistent with eight Cl atoms.

Chloro(2-oxa-3-oxotetrakis(2,6-dichlorophenyl)porphinato)iron(III) |Fe^{III}(Cl) 2|. The chloroiron complex was obtained quantitatively by refluxing the metal-free base with ferrous chloride ($^{57}FeCl_2$ for Mössbauer spectroscopy)[16,22] in DMF. ^{1}H NMR (500 MHz, chloroform-*d*): 88.2, 84.5, 83.3, 81.6, 74.9, 73.0 (bs, 1:1:1:1:1:1 H, py-H), 14.95, 14.65, 13.5, 12.0 (s, 1:1:4:2 H, phenyl *m*-H) ppm. HRMS (FAB): *m/z* calcd for $C_{43}H_{18}N_4Cl_8O_2Fe$ 959.8320, found 959.8257. Anal. Calcd for $C_{43}H_{18}N_4Cl_9O_2Fe$: C, 51.77; H, 1.81; N, 5.61; Fe, 5.59. Found: C, 51.95; H, 1.81; N, 5.42; Fe, 5.29.

Metathesis of Chloroiron(III) Complexes. Hydroxo complexes |Fe^{III}(OH) **1**| and |Fe^{III}(OH) **2**| were generated by percolating methylene chloride solutions of the chloro complexes through basic alumina. Trifluoromethanesulfonate (triflate) complex |Fe^{III}(Tf) **2**| was obtained from the hydroxo complex by treating a methylene chloride solution with a slight excess of triflic anhydride and evaporating the volatiles under reduced pressure.

Table 1. X-ray Experimental Data

formula	$C_{43}H_{18}N_4O_2Cl_9Fe$
molecular weight	997.6
color	dark blue
cryst syst	monoclinic
a (Å)	17.433(5)
b (Å)	15.099(4)
c (Å)	18.023(5)
β (deg)	92.23(2)
V (Å^3)	4740.4
Z	4
D_{calc} (g cm^{-3})	1.398
wavelength (Å)	0.7107
μ (cm^{-1})	8.668
space group	$P2_1/n$
diffractometer	Enraf-Nonius CAD4-F
cryst dimens (mm)	045 × 0.40 × 0.38
temp, °C	20
radiation	Mo Kα (graphite monochromated)
mode	$\theta/2\theta$
scan speed	variable
scan width (deg)	1.41 + 0.34 tan(θ)
octants	$+h+k\pm l$
θ(min/max) (deg)	2/26
no. of data collected	10 315
no. of data with $I > 3\sigma(I)$	3870
no. of variables	532
abs min/max	0.98/1.00
$R(F)$	0.080
$R_w(F)$	0.087
p	0.08
largest peak in final diff map (e Å^3)	0.20
GOF	1.597

Oxidation Reactions. Compound I analogues were generated at −80 °C by oxidation of |Fe^{III}(Cl) **1**| or |Fe^{III}(Tf) **2**| in 9:1 methylene chloride/methanol-d_4 with 2 equiv of *m*-CPBA in methanol-d_4. Mössbauer samples of |Fe^{IV}=O **1**|$^+$ and |Fe^{IV}=O **2**|$^+$ were generated in toluene and butyronitrile, respectively. Because of the lower stability of the compound I analogues in these solvents, the Mössbauer spectra were contaminated with the reduced oxoferryl and ferric complexes. Compound II analogues were generated by oxidation of |Fe^{III}(OH) **1**| with *m*-CPBA in THF. The specific procedures for generating UV−vis, NMR, Mössbauer, EPR, and resonance Raman samples were similar to those reported for high-valent porphyrins.[16]

X-ray Experimental Section. Suitable single crystals of |Fe^{III}(Cl) **2**| were obtained by slow diffusion of pentane into methylene chloride solutions of the complex. Systematic searches in reciprocal space using a Nonius Mach 3 automatic diffractometer showed that the crystals of |Fe^{III}(Cl) **2**| belong to the monoclinic system, space group $P2_1/n$. The unit-cell dimensions and their standard deviations were obtained and refined at 20 °C with Mo Kα radiation ($\lambda = 0.7107$ Å) using 18 selected reflections. Table 1 reports X-ray experimental details and results.

Single crystals of 0.45 × 0.40 × 0.38 mm^3 were cut from a cluster of crystals, glued to the end of a glass fiber, and mounted on a rotation-free goniometer head. All quantitative data were obtained at 20 °C using graphite-monochromated radiation; 10 316 ($+h+k\pm l$) reflections were recorded ($2° < \theta < 26°$). The resulting data set was transferred to a DEC-AZP3600S computer. For all subsequent calculations, the Nonius Molen package[24] was used.

Three standard reflections measured hourly during the data collection period showed no significant trend. Data were corrected for Lorentz and polarization factors. A unique data set of 3870 reflections having $I > 3\sigma(I)$ was used for determining and refining the structure. The structure was solved using direct methods. After refinement of all the non-hydrogen atoms, the difference Fourier map revealed maxima of

(23) Crossley, M. J.; King, L. G. *J. Chem. Soc., Chem. Commun.* **1984**, 920−922.

(24) Fair, C. K. In *Molen. An Interactive Intelligent System for Crystal Structure Analysis*; Nonius: Delft, The Netherlands, 1990.

Table 2. Electronic Spectra of Porpholactone Metal-Free Bases and Chloroiron(III) Complexes

compd	λ_{max} (nm) (ϵ ($mmol^{-1}$ cm^2)) Soret	vis
$\|H_2$ **1**$\|$	418 (428.5)	519 (19.77), 556 (20.80), 587 (12.77), 641 (8.94)
$\|H_2$ **2**$\|$	417 (430.8)	516 (24.26),552 (18.11), 590 (11.43), 645 (21.87)
$\|H_2$ TMP$\|$	418 (417.0)	514 (17.82), 547 (5.38), 588 (5.35), 645 (2.50)
$\|H_2$ TDCPP$\|$	418 (455.4)	512 (33.07), 588 (10.11), 6.46 (0.59)
$\|H_2$ 2,3-$(OH)_2$-2,3-Me_2-TMC$\|$	418 (215.5)	521 (18.11), 547 (16.25), 599 (8.48), 652 (41.61)
$\|H_2$ 2,3-$(OH)_2$-2,3-Me_2-TDCPC$\|$	414(157.1)	517 (14.32), 543 (7.82), 606 (6.02), 661 (36.43)
$\|Fe^{III}$(Cl) **1**$\|$	389 (24.75), 421 (34.49)	564 (5.03), 693 (1.40)
$\|Fe^{III}$(Cl) **2**$\|$	382 (34.04), 418 (55.38)	571 (7.05), 689 (3.14)
$\|Fe^{III}$(Cl) TMP$\|$	376 (49.57), 419 (93.76)	510 (12.11), 577 (3.06), 694 (2.50)
$\|Fe^{III}$(Cl) TDCPP$\|$	365 (41.72), 417 (89.93)	508 (10.93), 643 (3.60)
$\|Fe^{III}$(Cl) 2,3-$(OH)_2$-2,3-Me_2-TMC$\|$	380 (40.06), 414 (43.57)	595 (11.15)

residual electronic density close to the positions expected for hydrogen atoms. These were introduced into structure factor calculations as fixed contributors (C−H = 0.95 Å) and isotropic temperature factors such as $B(H) = 1.3B_{eqv}(C)$ Å^2. Full least-squares refinements against $|F|$ converged to $R(F) = 0.080$ and $R_w(F) = 0.087$ ($w - 1/\sigma(F^2)$, $\sigma^2(F^2) = \sigma^2$ counts + (pI^2). Final difference maps revealed no significant maxima. The scattering factor coefficients and anomalous dispersion coefficients come from ref 25.

Results

Electronic Spectra. The far-red visible band in the electronic spectra of $|H_2$ **1**$|$ and $|H_2$ **2**$|$ (Table 2) shows behavior characteristic of partially saturated porphyrin macrocycles,[26] undergoing a bathochromic shift and an increase in intensity, relative to porphyrin spectra. The Q_0-band of high-spin $|Fe^{III}$(Cl) **1**$|$ and $|Fe^{III}$(Cl) **2**$|$ behaves in parallel fashion, with an intense visible band red-shifted relative to high-spin chloroiron(III) *meso*-tetraarylporphyrins.

Oxidation of $|Fe^{III}$(Cl) **1**$|$ and $|Fe^{III}$(Tf) **2**$|$ with *m*-CPBA yields brown-green solutions, in contrast to the characteristically bright-green solutions of compound I analogues obtained from porphinatoiron complexes.[16,27] The dominant features of the electronic spectra are a broad band at ∼400 nm in the Soret region with markedly decreased intensity compared to the Soret bands of the starting complexes and the appearance of a second broad, low-intensity band between 730 and 745 nm (Figure 1). This band appears between the wavelengths of the radical marker bands of compound I complexes of *meso*-tetraarylporphyrins and -chlorins.[28−30]

Electrochemistry. $|H_2$ **1**$|$, $|H_2$ **2**$|$, and the chloroiron(III) complexes $|Fe^{III}$(Cl) **1**$|$ and $|Fe^{III}$(Cl) **2**$|$ undergo reversible one-electron oxidations at $E^{ox}_{1/2}$ values given in Table 3, in which oxidation potentials are compared to those of metal-free bases and chloroiron(III) complexes of *meso*-substituted tetramesityl- and tetrakis(2,6-dichlorophenyl)porphyrins and *meso*-tetramesitylchlorins. The first oxidation potential of the porpholactone bases and chloroiron(III) complexes is anodic relative to that of the corresponding porphyrins, in contrast to the first oxidation potential of chlorin bases and chloroiron(III) complexes, which show a cathodic shift.[30]

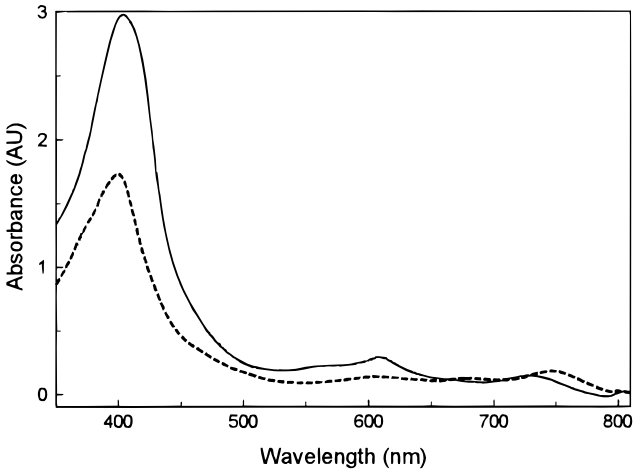

Figure 1. UV−vis spectra of compound I analogues (methylene chloride/methanol-d_4, −80 °C) of $|Fe^{IV}$═O **1**$|^+$ (dashed line) (λ_{max} ($\epsilon \times 10^{-3}$ $mmol^{-1}$ cm^2) 404 (20.52), 604 (1.54), 681 (1.37), 744 (2.08) nm) and $|Fe^{IV}$═O **2**$|^+$ (solid line) (λ_{max} ($\epsilon \times 10^{-3}$ $mmol^{-1}$ cm^2) 406 (24.84), 730 (1.05) nm). The band at ∼610 nm in the spectrum of $|Fe^{IV}$═O **2**$|^+$ represents a small quantity of ferryl impurity.

Table 3. Oxidation Potentials of Porpholactones Compared to Those of Porphyrins and Chlorins Having Identical *meso*-Phenyl Substituents[a]

compd	$E^{ox}_{1/2}$ (V)
$\|H_2$ **1**$\|$	+1.12
$\|H_2$ TMP$\|$	+0.90
$\|Fe^{III}$(Cl) **1**$\|$	+1.19
$\|Fe^{III}$(Cl) TMP$\|$	+0.915
$\|H_2$ 2,3-$(OH)_2$-2,3-Me_2-TMC$\|$	+0.91
$\|Fe^{III}$(Cl) 2,3-$(OH)_2$-2,3-Me_2-TMC$\|$	+1.046
$\|H_2$ **2**$\|$	+1.37
$\|H_2$ TDCPP$\|$	+1.25
$\|Fe^{III}$(Cl) **2**$\|$	+1.37
$\|Fe^{III}$(Cl) TDCPP$\|$	+1.30

[a] Methylene chloride; 0.1 M $Bu_4N^+PF_6^-$ electrolyte, scan rate 200 mV s^{-1}.

^{1}H NMR. In the ^{1}H NMR spectra of $|H_2$ **1**$|$ and $|H_2$ **2**$|$, absence of a symmetry element is apparent in the resolution of six unique pyrrole β-H resonances and two pyrrole N*H* protons. The pyrrole N*H* signals have been assigned to the most stable tautomer on the basis of a published iterative extended Hückel (IEH) calculation,[13] which is the *trans* tautomer not involving the oxazolone ring. The hyperfine shifts of the inequivalent N*H* proton resonances are −1.9 and −1.5 ppm for both metal-free bases, downfield of typical porphine shifts (∼2.5 ppm), suggesting that the ring currents of the porpholactones are smaller. The pattern of contact shifts of the pyrrole β-proton resonances of the chloroiron(III) complexes $|Fe^{III}$(Cl) **1**$|$ and $|Fe^{III}$(Cl) **2**$|$ (Figure 2) is less anisotropic than that of high-spin

(25) Cromer, D. T.; Waber, J. T. *International Tables for X-ray Crystallography*; The Kynoch Press: Birmingham, England, 1974; Vol. IV, (a) Table 2.2b, (b) Table 2.3.1.
(26) Gouterman, M. In *The Porphyrins*; Dolphin, D., Ed.; Academic Press: New York, 1978; Vol. III, pp 1−165.
(27) Groves, J. T.; Haushalter, R. C.; Nakamura, M.; Nemo, T. E.; Evans B. J. *J. Am. Chem. Soc.* **1987**, *103*, 2884−2886.
(28) Ozawa, S.; Watanabe, Y.; Morishima, I. *Inorg. Chem.* **1992**, *31*, 4042−4043.
(29) Ozawa, S., Watanabe, Y.; Morishima, I. *J. Am. Chem. Soc.* **1994**, *116*, 5832−5838.
(30) Jayaraj, K.; Gold, A.; Austin, R. N.; Mandon, D.; Weiss, R.; Terner, J.; Bill, E.; Müther, M.; Trautwein, A. X. *J. Am. Chem. Soc.* **1995**, *117*, 9079−9080.

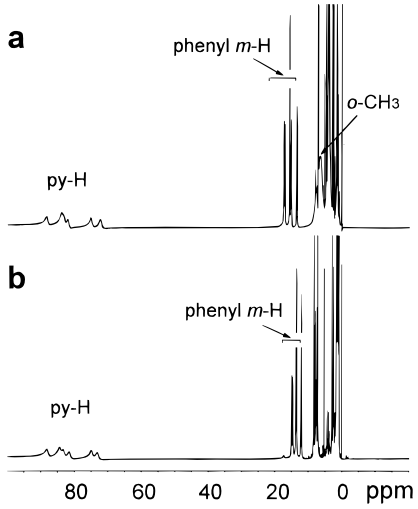

Figure 2. Ambient temperature ^{1}H NMR spectra (500 MHz, chloroform-*d*) of (a) |Fe^{III}(Cl) **1**| and (b) |Fe^{III}(Cl) **2**|. Signals are identified on traces.

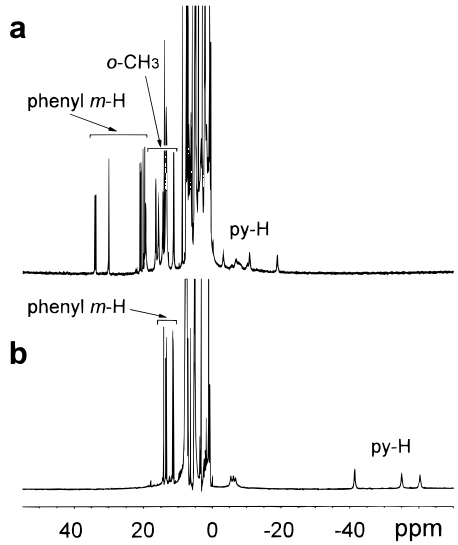

Figure 3. ^{1}H NMR (500 MHz, methylene-d_2 chloride, −70 °C) of (a) |Fe^{IV}═O **1**|$^+$ and (b) |Fe^{IV}═O **2**|$^+$. Resonances are identified on traces; signals at ∼−6 ppm arise from some decomposition because of warming of the NMR tube during transfer to probe.

ferric tetraarylchlorins.[30] However, the lack of a symmetry element remains evident in resolution of all six pyrrole proton resonances.

The pyrrole proton signals of |Fe^{IV}═O **1**|$^+$ and |Fe^{IV}═O **2**|$^+$ are shifted upfield of TMS, and phenyl meta proton signals are shifted downfield (Figure 3). Although the pyrrole proton signals display considerable anisotropy, the anisotropy is less pronounced than that observed for the pyrrole signals in the ^{1}H NMR spectra of the compound I complexes of *meso*-tetraarylchlorin complexes.[30] The pyrrole proton resonances of |Fe^{IV}═O **2**|$^+$ are grouped ∼20 ppm upfield from those of |Fe^{IV}═O **1**|$^+$. The situation is reversed for the phenyl meta-proton resonances, which are shifted further downfield for |Fe^{IV}═O **1**|$^+$ than for |Fe^{IV}═O **2**|$^+$.

EPR and Mössbauer Spectroscopy. The first-derivative EPR spectra of the starting complexes |Fe^{III}(Cl) **1**| and |Fe^{III}-(Cl) **2**| in frozen methylene chloride solution are typical of those of axial high-spin ferric complexes,[31] with effective *g* values close to 6.0 and 2.00, while the EPR spectrum of |Fe^{III}(Tf) **2**|

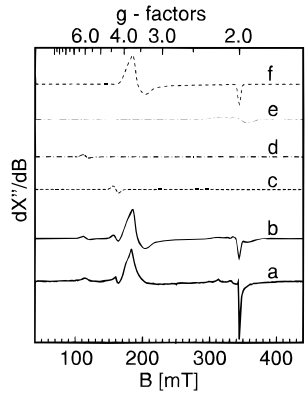

Figure 4. X-band absorption derivative EPR spectra of |Fe^{IV} ═O **1**|$^+$ in frozen toluene. The oxidized complexes were generated with *m*-CPBA. (a) Experimental spectrum recorded at 10 K with 9.6456 GHz microwave frequency at 20 mW microwave power, modulation amplitude 0.5 mT, modulation frequency 100 kHz. (b) Superposition of the simulated traces c−f. (c) Simulation of rhombic ferric high-spin contamination (decomposed macrocycle) with isotropic effective *g* value g^{eff} = 4.3 (0.5% relative intensity). (d) Simulation of ferric starting material with effective *g* values $\mathbf{g}^{eff}$ = (6.0, 6.0, 2.0) (3.5% relative intensity). (e) Simulation of ferric low-spin species with effective *g* values $\mathbf{g}^{eff}$ = (1.95, 1.95.0, 2.2), (10.6% relative intensity). (f) Spin-Hamiltonian simulation for |Fe^{IV} ═O **1**|$^+$ using the parameters of Table 4 (85.5% relative intensity).

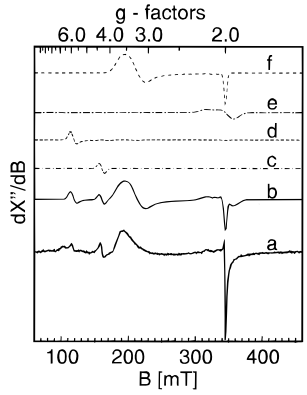

Figure 5. X-band absorption derivative EPR spectra of |Fe^{IV} ═O **2**|$^+$ in frozen butyronitrile. The oxidized complexes were generated with *m*-CPBA. (a) Experimental spectrum recorded at 4.2 K with 9.6420 GHz microwave frequency at 20 mW microwave power, modulation amplitude 1 mT, modulation frequency 100 kHz; (b) Superposition of the simulated traces c−f. (c) Simulation of rhombic ferric high-spin contamination (decomposed macrocycle) with isotropic effective *g* value g^{eff} = 4.3 (1.5% relative intensity). (d) Simulation of ferric starting material with effective *g* values $\mathbf{g}^{eff}$ = (5.8, 5.8, 2.0) (3.0% relative intensity). (e) Simulation of ferric low-spin species with effective *g* values $\mathbf{g}^{eff}$ = (1.95, 1.95, 2.18) (12.5% relative intensity). (f) Spin-Hamiltonian simulation for |Fe^{IV} ═O **2**|$^+$ using the parameters of Table 4 (83% relative intensity).

in frozen butyronitrile shows slight rhombicity and corresponds to a quantum mechanically admixed $S = {}^5/_2, {}^3/_2$ species,[31,32] having effective *g* values close to 5.94, 5.82 and 1.994 (not shown). Oxidations of methylene chloride/methanol-d_4 or toluene/methanol-d_4 solutions of |Fe^{III}(Cl) **1**| and butyronitrile solutions of |Fe^{III}(Tf) **2**| led to strong attenuation of the ferric high-spin signals in the spectra with concomitant appearance of new resonances from the oxidation product at g^{eff} = 3−4 and 2 (Figures 4a, 5a). The *g* factors indicate spin quartet species and therefore confirm ferromagnetic coupling of ferryl (*S* = 1) iron to the porpholactone π-cation radical. The spectra

(31) Palmer, G. In *Iron Porphyrins, Part II*; Lever, A. B. P., Gray, H., Eds.; Addison-Wesley Publishing Co.: Reading, MA, 1983; pp 43−88.

(32) Reed, C. A.; Mashiko, T.; Bentley, S. P.; Kastner, M. E.; Scheidt, W. R.; Spartalian, K.; Lang, G. *J. Am. Chem. Soc.* **1979**, *101*, 2948−2958.

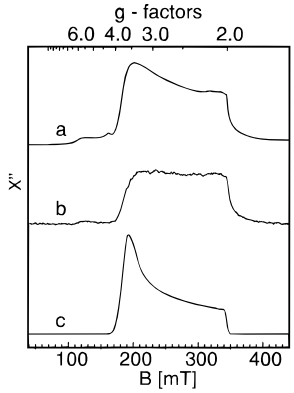

Figure 6. X-band EPR absorption spectra of $|Fe^{IV}=O\ \mathbf{1}|^+$ in frozen toluene: (a) obtained by numerical integration of the absorption derivative spectrum shown in Figure 4a; (b) recorded in the disperion mode at 1.8 K under rapid passage conditions with 20 μW microwave power at 9.6437 GHz, modulation frequency 100 kHz, modulation amplitude 0.1 mT, sweep rate 7.8 mT/s; (c) spin-Hamiltonian simulation for $|Fe^{IV}=O\ \mathbf{1}|^+$ using the parameters of Table 4.

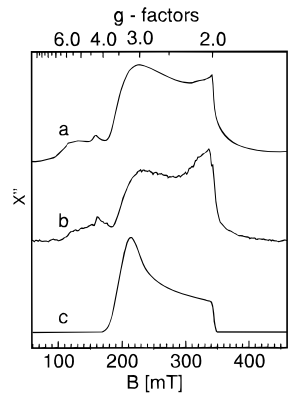

Figure 7. X-band EPR absorption spectra of $|Fe^{IV}=O\ \mathbf{2}|^+$ in frozen butyronitrile: (a) obtained by numerical integration of the absorption derivative spectrum shown in Figure 5a; (b) recorded in the disperion mode at 4.2 K under rapid passage conditions with 20 mW microwave power at 9.6424 GHz, modulation frequency 100 kHz, modulation amplitude 1 mT, sweep rate 19.5 mT/s; (c) spin-Hamiltonian simulation for $|Fe^{IV}=O\ \mathbf{2}|^+$ using the parameters of Table 4.

show some contamination of the oxidized samples with decomposed material ($g^{eff} = 4.3$), Fe(III) low-spin species ($g = 2.2-1.95$), and traces of organic radical ($g = 2.0$, narrow line). For spin quantitation the EPR spectra were simulated (Figure 4b−f, 5b−f) and the subspectra separately double-integrated. Comparison with the ferric starting complexes reveals that >50% of the spins initially present are converted to the quartet species with the remainder being EPR-inactive. The Mössbauer data below show that the balance is the $S = 1$ compound II analogue, accounting for 40% in the case of $|Fe^{IV}=O\ \mathbf{1}|$ and 49% in the case of $|Fe^{IV}=O\ \mathbf{2}|$, consistent with the EPR quantifications. Relative intensities of the subspectra are given in the figure captions. In Figures 6 and 7, the numerically integrated first-derivative traces are compared with quasi-absorption spectra recorded under rapid passage conditions in the dispersion mode to demonstrate that the EPR signals do, in fact, represent the derivative spectra of a "$S_t = {}^3/_2$" system. The major absorption in these spectra clearly extends from $g^{eff} = 3-4$ to 2, with the absorption maximum in the "$g_\perp$" region at about $B = 200-300$ mT and a decline of intensity toward $g_{||} \approx 2$, as expected for the resonances from the energetically isolated ground state Kramers doublets $|{}^3/_2, \pm{}^1/_2\rangle$ of a spin system $S_t = {}^3/_2$ in frozen solution with $E/D \approx 0$. The edges of the spectra are overlapping with the contributions from the contaminants mentioned above. Nevertheless, the absorption representations give an instructive overview of the spectra of the oxidized samples since the peak areas, apart from a g-dependent correction factor,[18] directly represent spectral intensities.

To obtain a first estimate of the spin-Hamiltonian parameters, we made use of the inherent correlation of effective EPR g values with the ratio $J/|D|$.[33] The values of $J/|D|$ obtained this way from the experimental data are in the range 0.7−1.0 for $|Fe^{IV}=O\ \mathbf{1}|^+$ and 0.3−0.7 for $|Fe^{IV}=O\ \mathbf{2}|^+$. The unusual line shapes in absorption-derivative as well as dispersion-mode spectra of $|Fe^{IV}=O\ \mathbf{1}|^+$ and $|Fe^{IV}=O\ \mathbf{2}|^+$ suggest strong angular variation of spin-packet line widths depending on the orientation of resonance fields within the molecular axis systems. On the basis of observations in other synthetic and biological compound I species,[7,16,17] we attribute the line width variations to inhomogeneous distributions of spin-Hamiltonian parameters. Simulations based on this assumption provide reasonable fits to the measured data (Figures 4b,f, 5b,f), for which the specific line shapes of the simulated powder spectra were obtained by adopting Gaussian distributions for the rhombicity parameter E/D and the isotropic coupling constant, J_0. The (mean) values of the spin Hamiltonian parameters used for the simulations (Table 4) were derived in conjunction with the analyses of magnetic Mössbauer spectra described below.

Mössbauer spectra of $|Fe^{IV}=O\ \mathbf{1}|^+$ in toluene/methanol-d_4 and $|Fe^{IV}=O\ \mathbf{2}|^+$ in butyronitrile were measured at varying temperatures and magnetic fields. The low-temperature spectra of *m*-CPBA-oxidized $|Fe^{IV}=O\ \mathbf{1}|^+$ shown in Figure 8 are representative of those of meso-substituted oxoiron(IV) π-cation radical porphyrin analogues.[16] The four-line pattern results from the combined effect of ferryl iron quadrupole splitting and "$S_t = 3/2$" magnetic hyperfine interaction. The spectra of the oxoferryl cation radical $|Fe^{IV}=O\ \mathbf{1}|^+$ could be simulated on the basis of the spin-Hamiltonian formalism. Most relevant to the determination of the electronic spin Hamiltonian parameters is that the influence of the perturbing magnetic field could be reproduced over a wide range of applied fields. Spin relaxation at 4.2 K and below was assumed to be slow with respect to nuclear precession time of about 10^{-8} s. As the magnetic hyperfine interactions are less sensitive to small variations in rhombicity and exchange coupling than EPR transitions, the distributions of E/D and J_0 were neglected for the Mössbauer simulations at the expense of only minor misfits in the line shapes. The minor contribution of the ferric contaminants was also not taken into consideration in the Mössbauer analyses. However, in order to simulate the spectra of the oxoferryl radical cation $|Fe^{IV}=O\ \mathbf{1}|^+$ accurately, it was necessary to superimpose contamination by the neutral oxoferryl compound II analogue $|Fe^{IV}=O\ \mathbf{1}|^0$ accounting for about 40% of the total iron, with spin-Hamiltonian parameters $D = 20$ cm^{-1}, $E/D = 0.$, $\mathbf{g} = (2.170, 2.17, 1.99)$, $\Delta E_Q = 1.80$ mm s^{-1}, $\delta = 0.08$ mm s^{-1}, $\mathbf{A}/g_N\mu_N = (-22.0, -22.0, -10.0)$ T. These values closely resemble those of the radical complex. This similarity is corroborated by the zero-field spectrum at 77 K of the oxidized sample, which shows a single quadrupole doublet (data not shown).

The field-dependent spectra of *m*-CPBA-oxidized $|Fe^{III}$ (Tf) $\mathbf{2}|$ (Figure 9b,c) could not be simulated by a single "$S_t = {}^3/_2$" species $|Fe^{IV}=O\ \mathbf{2}|^+$. Superposition of subspectra from the compound II contaminant $|Fe^{IV}=O\ \mathbf{2}|^0$ and a minor component porpholactone with ferric iron ($S = {}^5/_2$) led to satisfactory simulations (Figure 9). The weak contribution of the ferric complex was readily determined from the lines resolved at high

(33) Rutter, R.; Hager, L. P.; Dhonau, H.; Hendrick, M.; Valentine, M.; Debrunner, P. *Biochemistry* **1984**, *23*, 6809−6816.

Table 4. Comparison of Spin-Hamiltonian and Mössbauer Parameters of Oxoferryl Porpholactone π-Cation Radical Complexes with Oxoferryl Porphyrin and Chlorin π-Cation Radical Complexes

	$\|Fe^{IV}{=}O\mathbf{1}\|^+$	$\|Fe^{IV}{=}O$ TMP$\|^+$ [f]	$\|Fe^{IV}{=}O\mathbf{2}\|^+$	$\|Fe^{IV}{=}O$ TDCPP$\|^+$ [f]	$\|Fe^{IV}{=}O$ 2,3-$(OH)_2$-tetramesitylchlorin$\|^+$ [g]
D (cm^{-1})	22 ± 2	25	20 ± 2	25	23
E/D	0.06[a]	0.04	0.1[c]	0.07	0.053
g	2.18, 2.20, 1.99	2.21, 2.23, 1.99	2.17, 2.17, 1.99	2.20, 2.24, 1.99	
ΔE_Q (mm s^{-1})	1.80 ± 0.01	1.62	1.66 ± 0.01	1.48	1.25
η	0.3	0	0.3	0	
δ (mm s^{-1})	0.08 ± 0.01	0.08	0.08 ± 0.01	0.06	0.07
$A_{XX}/g_N\mu_N$ (T)	−21.5	−25.0	−17.5	−24.5	−31.6
$A_{YY}/g_N\mu_N$ (T)	−21.5	−25.0	−17.5	−24.5	−27.4
$A_{ZZ}/g_N\mu_N$ (T)	−10	−5.0	−10.	−6.0	−10.0
J_0 (cm^{-1})	17[b]	43	11[d]	38	29.2
$\mathbf{J}^a$ (cm^{-1})	0.5, 0.5, −1.0	1.7, −3.4, 1.7	0.5, 0.5, −1.0	1.6, −3.2, 1.6	
$\mathbf{g}^{eff}$ [e]	3.48, 3.85, 1.99	4.47, 3.50, 1.98	3.16, 3.64, 1.99	4.26, 3.62, 1.98	3.80, 4.23, 2.02

[a] $\sigma(E/D) = 0.039$. [b] $\sigma(J_0) = 2$ cm^{-1}. [c] $\sigma(E/D) = 0.05$. [d] $\sigma(J_0) = 2$ cm^{-1}. The values $\sigma(x)$ represent the widths of the Gaussian distributions $(2\pi\sigma^2)^{-1/2} \exp(-x^2/2\sigma^2)$ of the distributed parameters x derived from the simulations of the EPR spectra. [e] Effective g values obtained from spin-Hamiltonian simulations of EPR spectra (see text). [f] The values for $|Fe^{IV}{=}O$ TMP$|^+$ and $|Fe^{IV}{=}O$ TDCPP$|^+$ are taken from ref 16. [g] The parameters for $|Fe^{IV}{=}O$ 2,3-$(OH)_2$-tetramesitylchlorin$|^+$ are taken from ref 30.

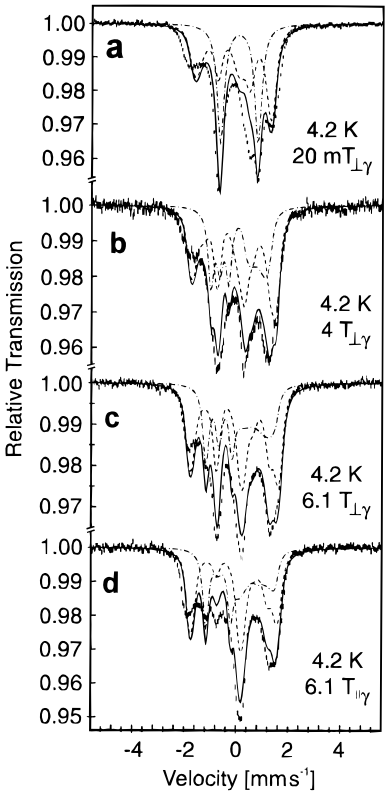

Figure 8. Magnetically perturbed Mössbauer spectra of $|Fe^{IV}{=}O\mathbf{1}|^+$ in toluene at 4.2 K with different fields applied perpendicular or parallel to the γ-rays. Solid lines represent the sums of the following subspectra: The dashed line (− − −) represents 60% $|Fe^{IV}{=}O\mathbf{1}|^+$ compound I analogue simulated with the parameters in Table 4. The dash-dotted line (− · −·) represents 40% $|Fe^{IV}{=}O\mathbf{1}|^0$ compound II analogue simulated with the parameters given in the text.

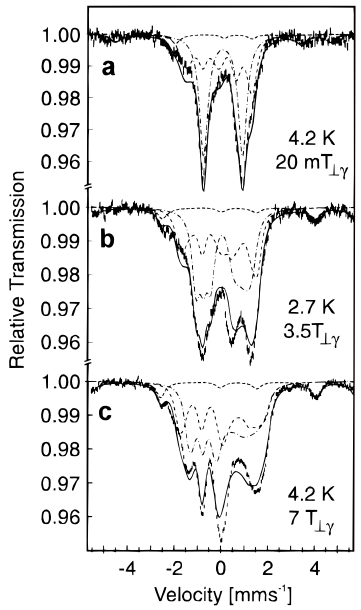

Figure 9. Magnetically perturbed Mössbauer spectra of $|Fe^{IV}{=}O\mathbf{2}|^+$ in butyronitrile at 4.2 and 2.7 K with different fields applied perpendicular to the γ-rays. Solid lines represent the sums of the following subspectra: The long-dashed line (− − −) represents 44% $|Fe^{IV}{=}O\mathbf{2}|^+$ compound I analogue simulated with the parameters in Table 4. The dash-dotted line (− · −·) represents 49% $|Fe^{IV}{=}O\mathbf{1}|^0$ compound II analogue simulated with the parameters given in the text. The small-dashed line (- - -) is 9% ferric starting compound simulated with $S = 5/2$, $D = 8$ cm^{-1}, $E/D = 0.0$, $\mathbf{g} = (2, 2, 2)$, $\Delta E_Q = 1.45$ mm s^{-1}, $\delta = 0.40$ mm s^{-1}, $\mathbf{A}/g_N\mu_N = (-19, -19, -19)$ T.

and low velocities beyond ± 3 mm s^{-1}. The contaminant $|Fe^{IV}{=}O\mathbf{2}|^0$ ($S = 1$, $D > 0$) exhibits magnetic splitting only in moderate or strong fields. By contrast, the subspectrum of the target compound $|Fe^{IV}{=}O\mathbf{2}|^+$ (half-integer spin, $D > 0$) shows magnetic hyperfine splitting even in the low applied field of 20 mT, giving rise to the shoulders at +1.2 and −1.5 mm s^{-1} in the top panel of Figure 9. As in the case of the tetramesityl complex, the parameters for ferryl iron in $|Fe^{IV}{=}O\mathbf{2}|^0$, D = 20 cm^{-1}, $E/D = 0.1$, $\mathbf{g} = (2.17, 2.17, 1.99)$, $\Delta E_Q = 1.66$ mm s^{-1}, $\delta = 0.08$ mm s^{-1}, $\mathbf{A}/g_N\mu_N = (-17.5, -17.5, -10.0)$ T, are similar to those of the radical complex (Table 4).

Resonance Raman Spectroscopy. Resonance Raman spectra (406.7 nm excitation) of the Fe^{III}(Tf) complexes of **1** and **2** and their oxidized derivatives are shown in Figures 10 and 11 with band assignments summarized in Table 5. The anomalously polarized a_{2g} modes listed in Table 5 which appear in the data shown in Figures 10 and 11 are consistent with the hyperporphyrin nature (red-shifted Soret bands)[34] of the iron porpholactone absorptions. In order to understand the porpholactone resonance Raman data we utilized the published vibrational mode analysis of Ni(II) octaethylchlorin[35] as a model for the symmetry-lowering effects and decreased aromaticity of the oxazolone ring in the porpholactones. We found that despite the replacement of a pyrrole with the oxazolone ring, the overall resonance Raman band patterns and skeletal mode

(34) Terner, J.; Topich, J. *Chem. Phys. Lett.* **1984**, *106*, 508−512.
(35) Prendergast, K.; Spiro, T. G. *J. Phys. Chem.* **1991**, *95*, 1555−1563.

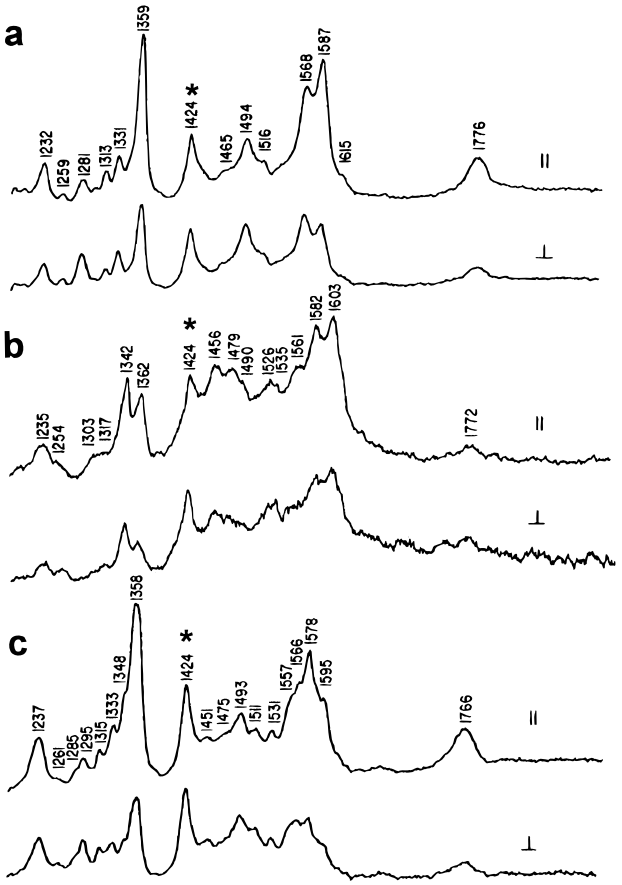

Figure 10. Resonance Raman data with 406.7 nm excitation (15 mW) for the 1230−1800 cm^{-1} region at −80 °C for (a) |Fe^{III}(Cl) **1**| in methylene chloride (1.0 mL); (b) the same compound as in part a after addition of a 2-fold molar excess of *m*-CPBA in methanol-d_4 (0.2 mL) and formation of the oxoferryl porpholactone π-cation radical; and (c) the Fe(IV) complex generated from |Fe^{III}(OH) **1**| in methylene chloride (1 mL) by the addition of a 2-fold molar excess of *m*-CPBA in THF (0.2 mL). Solvent bands are indicated by asterisks (*).

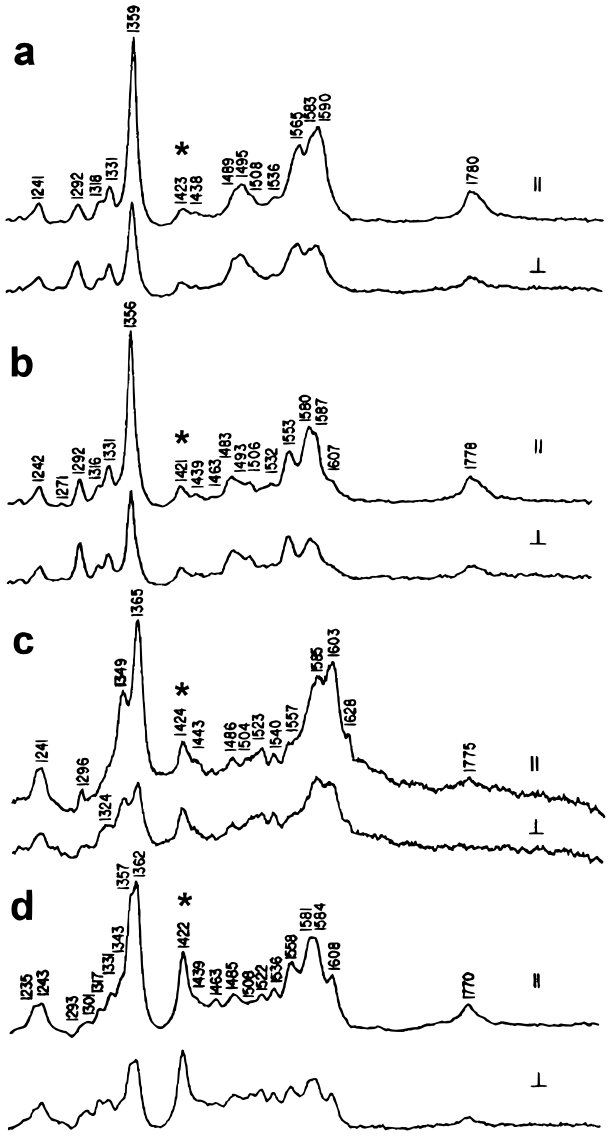

Figure 11. Resonance Raman data with 406.7 nm excitation (15 mW) for the 1230−1800 cm^{-1} region at −80 °C for (a) |Fe^{III}(Tf) **2**| in methylene chloride; (b) the same compound as in part a, but immediately after addition of a 2-fold molar excess of *m*-CPBA in methanol-d_4, showing the formation of a six-coordinate high-spin intermediate species; (c) the same compound as in part b, but 5 min later, showing formation of the oxoferryl porpholactone π-cation radical, and (d) the Fe(IV) complex generated from |Fe^{III}(OH) **2**| in methylene chloride (1.0 mL) by the addition of a 2-fold molar excess of *m*-CPBA in THF (0.2 mL). Solvent bands are indicated by asterisks (*).

frequencies mimic those of their respective parent porphyrins to a significant extent. Mode localization, which has sometimes been invoked for chlorins,[36] does not appear to be a significant factor for the porpholactones. The expected symmetry lowering in the porpholactones relative to porphyrin is evidenced by the activation and splitting of E_u modes, as has been reported for asymmetrically substituted physiological hemes.[37−39] However in contrast to chlorins,[35] the symmetry is evidently not lowered to such a degree that anomalously polarized a_{2g} bands become depolarized; nor have we found indications that depolarized b_{1g} modes become polarized. The band assignments of Table 5 are thus listed as analogues of the metallotetraphenylporphyrin Raman and infrared active modes, and they follow the numbering system used for Ni tetraphenylporphine.[40]

The resonance Raman spectra of the ferric porpholactone complexes shown in Figures 10a and 11a are dominated by a strong polarized ν_4 (a_{1g}) band near 1360 cm^{-1}. This frequency would be quite low for ν_4 bands of ferric porphyrin complexes and is in fact reminiscent of values normally observed for ferrous porphyrins.[39] However, treatment of |Fe^{III}(Tf) **1**| with sodium dithionite by shaking in a two-phase mixture of water and methylene chloride under N_2 causes ν_4 to shift down to 1340 cm^{-1}, consistent with a ferric-to-ferrous reduction. In the oxoferryl and oxoferryl porphyrin π-cation radical derivatives, ν_4 spawns a prominent second polarized component which is clearly evident between 1340 and 1350 cm^{-1}. Such splitting in chlorins has been attributed to symmetry lowering.[35] However, ν_4 is the only well-isolated porpholactone band which exhibits such behavior. The apparent splitting might be more satisfactorily explained by diminished ν_4 intensities and appearance of overtones of a_{1g} symmetry which derive their intensity through vibrational interactions with ν_4. In the ferric porpholactone complexes an apparently depolarized band appears near 1565 cm^{-1} (Figures 10a and 11a). Computer-assisted deconvolution reveals that this band actually results from the

(36) Boldt, N. J.; Donohoe, R. J.; Birge, R. J.; Bocian, D. F. *J. Am. Chem. Soc.* **1987**, *109*, 2284−2298.
(37) Choi, C.; Lee, J. J.; Wei, Y. H.; Spiro, T. G. *J. Am. Chem. Soc.* **1983**, *105*, 3692−3707.
(38) Hu, S.; Smith, K. M.; Spiro, T. G. *J. Am. Chem. Soc.* **1996**, *118*, 12638−12646.
(39) Spiro, T. G. In *Iron Porphyrins, Part II*; Lever, A. P. B., Gray, H. B., Eds.; Addison-Wesley: Reading, MA, 1983; pp 89−159.
(40) Li, X-.Y.; Czernuscewicz, R. S.; Kincaid, J. R.; Su, Y. O.; Spiro, T. G. *J. Phys. Chem.* **1990**, *94*, 31−47.

Table 5. Resonance Raman Frequencies (cm^{-1}) for Skeletal Modes of the Iron Complexes of Porpholactones **1** and **2**

		tetramesityl lactone			tetrakis(2,6-Cl_2-phenyl) lactone			
mode	polarization	Fe^{III}Tf	Fe^{IV}=O^+	Fe^{IV}=O	Fe^{III}Tf	Fe^{III} 6−coord high-spin	Fe^{IV}=O^+	Fe^{IV}=O
$\nu_{C=O}$	p	1776	1772	1766	1780	1778	1775	1770
ν_{10}	dp					1607	1628	
ϕ_4	p	1615			1583	1580		1584
ν_{37a}	p	1587	1603	1595	1590	1587	1603	1608
ν_2	p	1568	1582	1578	1565	1553	1585	1581
ν_{19}	ap	1568			1565	1553		
ν_{37b}	dp			1566				1536
ν_{38a}	p		1561	1557	1536	1532	1557	1558
ν_{38b}	dp	1516	1535	1531			1540	1522
ϕ_5		1511		1511	1508	1506	1504	1508
ν_{11}	dp	1494	1526	1493	1495	1493	1523	1485
ν_{28}	dp	1465	1490	1451	1489	1483	1486	
ν_3	p		1479	1475		1463		1463
ν_{39}	dp	1436	1456	1451	1438	1439	1443	1439
CH_2Cl_2		1424	1424	1424	1423	1421	1424	1422
ν_4	p	1359	1362	1358	1359	1356	1365	1362
	p		1342	1348			1349	1343
ν_{41}	dp	1331	1317	1333	1331	1331		1331
	p	1313	1303	1315	1318	1316		1317
ν_{26}	ap	1281		1295	1292	1292		
		1259	1254	1261		1271		
ν_1	p	1232	1235	1237	1241	1242	1241	1243
$\nu_{Fe=O}$			830	835			836	834

superposition of overlapping ν_2 (polarized) and ν_{19} (anomalously polarized) bands. Phenyl mode ϕ_4 appears at 1615 cm^{-1} for |Fe^{III}(Tf) **1**|, but at 1583 cm^{-1} for |Fe^{III}(Tf) **2**| in accord with lowered ring frequencies of chlorinated phenyls.[41] Additional features characteristic of the resonance Raman spectra of the porpholactones are polarized bands observed near 1780 cm^{-1} (Figures 10 and 11) which are attributable to carbonyl stretching modes of the lactone functionality of the oxazolone ring.

Since artifacts might be introduced by the continuously developing reaction mixtures during the generation of oxidized complexes, we verified many of the singular aspects of the resonance Raman spectra of the oxidized derivatives using stable low-spin adducts (CO, cyanide and imidazole, etc.) of **1** and **2**. An unanticipated observation for the oxoferryl complexes was the appearance of the polarized A component of ν_{37} (*via* symmetry lowering from E_u), denoted ν_{37a}, at a frequency ∼10 cm^{-1} higher in **2** than **1**. Nevertheless, we verified this unusual behavior with the stable low-spin adducts, which exhibited similar upshifted ν_{37a} frequencies for complexes of **2** relative to **1**. The π-cation radical complexes spontaneously convert to mixtures containing ferryl and ferric forms within a matter of minutes. Resonance Raman spectra of the ferryl forms of **1** and **2** generated by *m*-CPBA oxidation of their respective hydroxo complexes are given in Figures 10c and 11d.

Band assignments for the π-cation radical resonance Raman spectra are based on correlation with assignments for oxoferryl tetraarylporhyrin π-cation radicals.[42−44] Oxidation of the Fe^{III}-(Tf) complexes of **1** and **2** to their respective compound I analogues is accompanied by band broadening, frequency shifts, and decreases in intensity (Figures 10b, 11c), as previously observed for porphyrin π-cation radicals.[42−44] The ν_2 and ν_{11} mode analogues of |Fe^{IV}=O **1**|$^+$ and |Fe^{IV}=O **2**|$^+$ experience substantial frequency upshifts relative to their parent ferric complexes. Polarized bands at ∼1340 and 1360 cm^{-1} assignable to ν_4 are similar in frequency and intensity to ν_4 bands of compound I analogues of porphyrins.[16,42,43] The oxazolone carbonyl bands shift slightly down in frequency relative to the ferric complexes, but slightly up in frequency compared to the ferryl complexes. It is interesting that the carbonyl bands are broadened, suggesting a multicomponent nature, despite there being only one carbonyl per molecular unit. This aspect of lactone carbonyl vibrational bands was in fact explored some years ago by Jones and co-workers.[45]

During the oxidation of |Fe^{III}(Tf) **2**| at −80 °C we observed a species for which the ν_{37}, ν_2, and ν_{11} bands are shifted down in frequency (Figure 11b) relative to those of |Fe^{III}(Tf) **2**| (Figure 11a), indicating formation of a high-spin hexacoordinate transient. This species progresses to the compound I analogue within a minute or two and is attributed to the triflate complex of **2** with *m*-CPBA transiently coordinated at the sixth axial position. Though too rapid to detect for |Fe^{III}(Tf) **1**| with our present experimental arrangement, we have in fact observed similar hexacoordinate high-spin transients for a number of porphyrin systems.

In lower-energy resonance Raman spectra of |Fe^{IV}=O **1**|$^+$, we located an isotope-sensitive band at 830 cm^{-1}, shifting to 797 cm^{-1} on oxidation with ^{18}O-labeled *m*-CPBA, attributable to $\nu_{Fe=O}$. Similarly |Fe^{IV}=O **2**|$^+$ exhibits an isotope-sensitive band at 836 cm^{-1} (shifting to 790 cm^{-1}) assignable to $\nu_{Fe=O}$. In methylene chloride/methanol medium, similar values of $\nu_{Fe=O}$ have been reported for compound I analogues of tetramesitylporphyrin[42] and dihydrodimethyl-*meso*-tetramesitylchlorin.[30]

For the oxoferryl complexes, ^{18}O-substitution causes a band at 835 cm^{-1} in the resonance Raman spectrum of |Fe^{IV}=O **1**| to shift to 801 cm^{-1}, while a band at 834 cm^{-1} for |Fe^{IV}=O **2**| shifts to 798 cm^{-1}. These bands, with frequencies similar to those of the Fe=O bands of the compound I analogues, are assigned as Fe=O vibrational bands of the compound II analogues.

Crystallography. Crystals of |Fe^{III}(Cl) **2**| contain one independent molecule per asymmetric unit; thus no particular

(41) Dollish, F. R.; Fateley, W. G.; Bently, F. F. *Characteristic Raman Frequencies of Organic Compounds*; Wiley: New York, 1974.
(42) Hashimoto, S.; Mizutani, Y.; Tatsuno, Y.; Kitagawa, T. *J. Am. Chem.* **1991**, *113*, 6542−6549.
(43) Kitagawa, T.; Mizutani, Y. *Coord. Chem. Rev.* **1994**, *135/136*, 685−735.
(44) Jayaraj, K.; Terner, J.; Gold, A.; Roberts, D. A.; Austin, R. N.; Mandon, D.; Weiss, R.; Bill, E.; Müther, M.; Trautwein, A. X. *Inorg. Chem.* **1996**, *35*, 1632−1640.
(45) Jones, R. N.; Angell, C. L.; Ito, T.; Smith, R. J. D. *Can. J. Chem.* **1959**, *37*, 2007−2022.

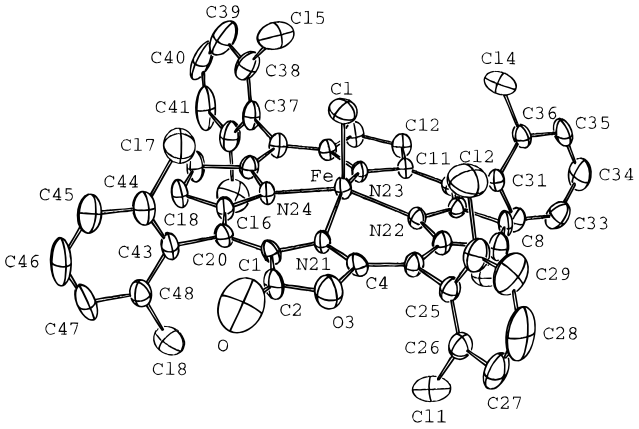

Figure 12. ORTEP plot of |Fe^{III}(Cl) **2**|.

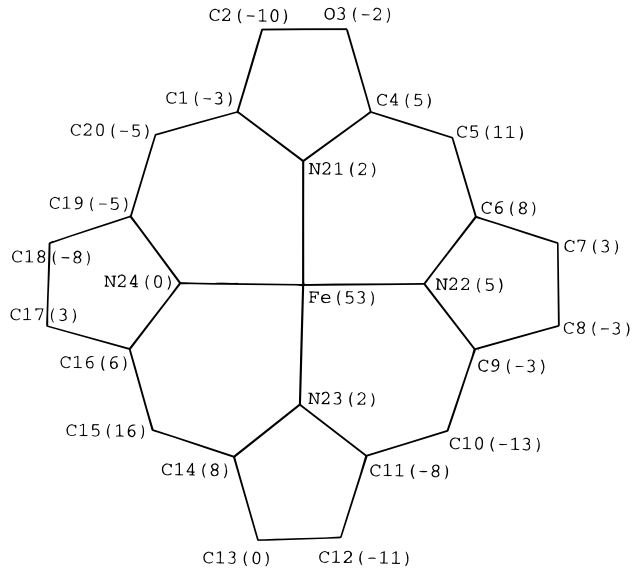

Figure 13. PLUTO plot of the 24-atom core projected onto the mean plane of the core. Numbers in parentheses indicate the deviation of atoms (in 0.01 Å units) with respect to the core mean plane.

symmetry is imposed on the complex. Figure 12 shows the ORTEP drawing of one |Fe^{III}(Cl) **2**| molecule while Figure 13 shows displacements of all of the porphyrin core atoms and the 3-oxo substituent relative to the 24-atom macrocycle mean plane in units of 0.01 Å. The conformation of the macrocycle of |Fe^{III}(Cl) **2**| is similar to that of zinc(II) tetrakis(2,6-dichlorophenyl)porphyrin.[46] In general, structural features of |Fe^{III}(Cl) **2**| are similar to those of high-spin iron porphyrins.[47] Iron is displaced 0.50(1) Å out of the pyrrole and oxazolone ring nitrogen mean plane in the direction of the axial chloro ligand, for which the Fe−Cl distance is 2.194(2) Å. The Fe−$N_{pyrrole}$ distances, which range from 2.051(4) to 2.074(3) Å, have a mean value of 2.062(3) Å, compared to the value of the Fe−$N_{oxazolone}$ bond length of 2.072(4) Å. These features indicate that the transformation of one of the pyrroles to an oxazolone ring introduces minimal asymmetry in the equatorial bonding of iron. Despite the 3-oxo substituent and the presence of an oxazolone ring in place of a pyrrole ring, the core of ligand **2** is nearly planar. A very small doming of the porpholactone ring conformation in |Fe^{III}(Cl) **2**| is indicated by the separation of 0.025(7) Å between the mean plane of the pyrrole and oxazolone ring nitrogens and the macrocycle core mean plane. Slight ruffling is indicated by the mean displacement of 0.114(8) Å of the meso carbons relative to the macrocycle core mean plane (Figure 13); however, the pyrrole and oxazolone rings are planar. The *meso*-phenyl substituents are oriented nearly perpendicular to the mean plane of the core, with dihedral angles ranging from 91.6(3) to 103.0(0)° (mean value 96.8(3)°). The *o*-chloro substituents of the phenyl rings form "pockets" 2.64 Å in depth on both faces of the mean plane of the core.

Discussion

The porpholactone macrocycle is distinguished from a porphyrin by substitution of an oxazolone ring for one of the pyrroles. This restricts π-conjugation around the periphery, but does not completely block the peripheral π-electron pathway as does saturation of a pyrrole $\beta-\beta$ bond in the case of the chlorin macrocycle. As a consequence, the porpholactone system is expected to have features in common with both porphyrins and chlorins. The consequences of restricted π-conjugation and lowered molecular symmetry on energies of the frontier molecular orbitals (MOs) of unsubstituted porpholactone have been predicted by an iterative extended Hückel (IEH) calculation.[13] The highest occupied molecular orbital (HOMO) of the porpholactone is stabilized and the next highest occupied molecular orbibtal destabilized relative to the corresponding porphine orbitals, the a_{2u} and a_{1u} MOs, respectively, under D_{4h} symmetry. The lowest unoccupied molecular orbitals (LUMOs) of porpholactone, correlating with the degenerate porphine 3e(π^*) MOs, split with the net result being a smaller HOMO−LUMO energy gap for porpholactone than for porphine. The effect of the decreased HOMO−LUMO separation on the electronic spectrum is a shift of the lowest energy Q-band to longer wavelengths with a concomitant gain in intensity relative to porphine.[26] The extent of these changes should, however, be less pronounced than for 2,3-dihydroporphine (chlorin free base). Comparison of the electronic spectra of |H_2 **1**| and |H_2 **2**| with the related porphine and chlorin bases bears out the IEH predictions (Table 2). Complexation of the porpholactone with iron does not change the qualitative orbital picture. Thus, the Q_0 band of the high-spin ferric complexes and the radical marker bands of |Fe^{IV}═O **1**|$^+$ and |Fe^{IV}═O **2**|$^+$ also exhibit similar behavior. The predicted stabilization of the porpholactone HOMO is also supported by the increase of first oxidation potentials of the metal-free bases and chloroiron(III) complexes relative to the corresponding tetraarylporphines and chloroiron(III) complexes (Table 3).

The shielding of the interior-ring proton resonances of porphines and related aromatic macrocycles is directly proportional to the magnitude of peripheral ring current. The N*H* signals of the porpholactone bases appear at shifts between porphyrins and chlorins consistent with a ring current of intermediate magnitude as expected from reduction of peripheral conjugation through the lactone function.[48] Resolution of two N*H* signals also confirms the absence of a symmetry element and an energy minimum associated with one tautomeric form that is predicted by the IEH treatment. Absence of a symmetry element is also evident in the anisotropy of the pyrrole proton signals in the high-spin iron(III) complexes, where all six proton resonances are resolved. However, anisotropy is less than that observed for the high-spin ferric chlorin complexes. Since the pyrrole hyperfine proton shifts of the high-spin ferric complexes

(46) Williamson, M. M.; Prosser-McCartha, C. M.; Mukundan, S.; Hill, C. L. *Inorg. Chem.* **1988**, *27*, 1061−1068.
(47) Scheidt, W. R.; Gouterman, M. In *Iron Porphyrins, Part I*; Lever, A. B. P., Gray, H., Eds.; Addison-Wesley Publishing Co.: Reading, MA, 1983; pp 89−139.
(48) Harel, Y.; Manassen, J. *Org. Magn. Reson.* **1981**, *15*, 1−6.

are predominantly contact in origin,[49] this observation suggests that electron density distribution in the molecular orbitals of the iron complexes, like that in the metal-free porpholactone bases, is less perturbed by the oxaxolone ring than by saturation of a pyrrole $\beta-\beta$ bond.

The general features of the ^{1}H NMR spectra of $|Fe^{IV}{=}O$ **1**$|^+$ and $|Fe^{IV}{=}O$ **2**$|^+$ are similar to those of compound I analogues of porphyrins and chlorins.[27,29,30] Contact shifts also dominate[49] contributions to the isotropic shifts of ring proton signals of the oxoferryl complexes of macrocycle π-cation radicals. Since the iron $d_{x^2-y^2}$ orbital is vacant in the porpholactone compound I analogues, unpaired spin distribution in the singly occupied π-type HOMO of the macrocycle is responsible for contact shifts. The porpholactone MO correlating with the a_{1u} porphyrin MO in the D_{4h} point group is expected to have large atomic orbital coefficients at the pyrrole α- and β-carbons and lactone group,[50] while the atomic orbital coefficients of the MO correlating with a_{2u} are largest at the macrocycle nitrogens and meso carbons. On the basis of the hyperfine shift patterns in the ^{1}H NMR spectra of $|Fe^{IV}{=}O$ **1**$|^+$ and $|Fe^{IV}{=}O$ **2**$|^+$ (Figure 3), the symmetry states of both porpholactone π-cation radicals are concluded to have considerable a_{1u} character as a result of an admixture of the frontier MOs. The decreased energy separation between the two highest occupied porpholactone MOs is a favorable situation for such admixture. The ^{1}H NMR data suggest that the admixture of a_{1u} character in $|Fe^{IV}{=}O$ **2**$|^+$ is greater than in $|Fe^{IV}{=}O$ **1**$|^+$. This inference is based on the larger hyperfine shifts of the pyrrole β proton signals of $|Fe^{IV}{=}O$ **2**$|^+$, which indicate larger unpaired spin at the β-carbons, consistent with increased $^2A_{1u}$ admixture. Stabilization of the a_{2u} MO by the electron-withdrawing 2,6-dichlorophenyl meso substituents[51] of $|Fe^{IV}{=}O$ **2**$|^+$ would be expected to increase in the proportion of $^2A_{1u}$ component in an $^2A_{1u}/^2A_{2u}$ admixture.[52]

The nature of the macrocycle radical in compound I analogues is reflected in the paramagnetic properties of the complexes since the exchange interaction between ferryl iron ($S = 1$) and porpholactone radical ($S' = {}^1/_2$) depends on the spin density at the equatorial nitrogens and radical localization on the lactone group associated with $^2A_{1u}$- and $^2A_{2u}$-like states.[53] Therefore low-temperature EPR and magnetically perturbed Mössbauer spectra of $|Fe^{IV}{=}O$ **1**$|^+$and $|Fe^{IV}{=}O$ **2**$|^+$ were recorded and analyzed within the spin-Hamiltonian formalism (eqs 1−3). To achieve unambiguous parametrizations the complementarity of the spectroscopic techniques was systematically utilized. The EPR spectra of $|Fe^{IV}{=}O$ **1**$|^+$ and $|Fe^{IV}{=}O$ **2**$|^+$ differ in appearance from those reported for compound I analogues of meso-substituted porphyrins[16] in that the signals exhibit nearly axial symmetry with strong variances of line widths. Narrow, very intense lines are observed in the $g_{||}^{eff}$ direction in contrast to broad lines in the $g_{\perp}^{eff}$ direction. However, as demonstrated in Figures 6 and 7, the major signals represent first-derivative spectra of a $S_t = {}^3/_2$ system. The 10% contribution of an $S = {}^1/_2$ species is corroborated both from the simulations of the first-derivative EPR signal and from the inspection of the absorption-type trace obtained in dispersion mode (Figures 6b, 7b). It is interesting to speculate that the origin of this signal may be explained by a broad asymmetric distribution of the coupling constant J with a tail reaching to negative values, the latter representing antiferromagnetic coupling of the spins of the Fe=O unit ($S = 1$) and the porpholactone radical ($S' = {}^1/_2$).

Assuming similar D values for the ferryl iron moieties in both compound I analogues, the smaller range of $J/|D|$ estimated for $|Fe^{IV}{=}O$ **2**$|^+$ than for $|Fe^{IV}{=}O$ **1**$|^+$ indicates weaker exchange coupling in $|Fe^{IV}{=}O$ **2**$|^+$, consistent with the observation based on NMR spectrometry of greater $^2A_{1u}$ character for $|Fe^{IV}{=}O$ **2**$|^+$. This conclusion is substantiated by the independent determination of D and J by Mössbauer spectroscopy.

The overall hyperfine splittings observed in the Mössbauer spectra of compound I analogues of *meso*-tetraarylporphyrins[16] and the tetramesitylchlorin[30] are about 25% larger than those observed in porpholactones (Figures 8, 9). The smaller splitting for the porpholactones is in qualitative accord with the EPR indication that ferromagnetic spin coupling in the oxidized porpholactones is weaker than that in the corresponding porphyrin analogues. The decreased splitting correlates with the reduced magnetic hyperfine interaction, with the latter indicating a reduced spin expectation value for the ground state electronic Kramers doublet due to stronger mixing of $S_t = {}^3/_2$ and $S_t = {}^1/_2$ spin multiplets. While the zero-field parameter $D = 22$ cm^{-1} is not very different from that of the Fe(IV)=O unit in porphyrins and the chlorin, the value $J_0 = 17$ cm^{-1} obtained for the exchange coupling constant of the porpholactone $|Fe^{IV}{=}O$ **1**$|^+$ is among the lowest found for meso-substituted porphyrin or chlorin analogues.[16] Figures 8 and 9 show that overall splitting for $|Fe^{IV}{=}O$ **2**$|^+$ is significantly smaller than that observed for $|Fe^{IV}{=}O$ **1**$|^+$. The estimated exchange coupling constant $J_0 = 11$ cm^{-1} is the smallest yet found for a compound I analogue of a porpholactone, chlorin, or meso-substituted or meso-unsubstituted pyrrole β-alkyl porphyrin.[54,55]

The small J values for $|Fe^{IV}{=}O$ **1**$|^+$ and $|Fe^{IV}{=}O$ **2**$|^+$ are consistent with the NMR data suggesting abstraction of an electron from an MO with a_{1u} character. This results in small electron spin density in the nitrogen orbitals and substantial spin density on the lactone group. The finding that J is smaller for $|Fe^{IV}{=}O$ **2**$|^+$ than for $|Fe^{IV}{=}O$ **1**$|^+$ is in accordance with the NMR result that the electron-withdrawing meso substituents in $|Fe^{IV}{=}O$ **2**$|^+$ enhance admixture of $^2A_{1u}$ character into the singly occupied MO, in contrast to the electron-releasing meso substituents of $|Fe^{IV}{=}O$ **1**$|^+$. Both the magnitude of $J/|D|$ and the qualitative appearance of the first-derivative EPR trace of $|Fe^{IV}{=}O$ **2**$|^+$ are similar to those of the $^2A_{1u}$ compound I analogue generated from the β-pyrrole octasubstituted porphyrin 2,7,12,17-tetramethyl-3,8,13,18-tetramesitylporphyrin[54,55] and of the compound I transients of ascorbate peroxidase[4] and *Micrococcus lysodeikticus* catalase.[7]

Of particular interest in the resonance Raman spectra of the compound I analogues of the porpholactones is the behavior of the "marker" bands ν_2 and ν_{11}, which have a strong component of $\beta-\beta$ stretch and are expected to show electronic symmetry state sensitivity. Because of nodes in the a_{1u} MO between the pyrrole β-carbons, the $C_\beta-C_\beta$ interaction is antibonding. The abstraction of an electron from the a_{1u} MO therefore increases $C_\beta-C_\beta$ bond strength, resulting in a shift up in frequency for modes containing $C_\beta-C_\beta$ components. By contrast, the $C_\beta-$

(49) Goff, H. M. In *Iron Porphyrins, Part I*; Lever, A. B. P., Gray, H., Eds.; Addison-Wesley Publishing Co.: Reading, MA, 1983; pp 237−281.
(50) Hanson, L. K.; Chang, C. K.; Davis, M. S.; Fajer, J. *J. Am. Chem. Soc.* **1981**, *103*, 663−670.
(51) Skillman, A. G.; Collins, J. R.; Loew, G. H. *J. Am. Chem*. Soc. **1992**, *114*, 9538−9544.
(52) Czernuszewicz, R. S.; Macor, K. A.; Li, X-.Y.; Kincaid, J. R.; Spiro, T. G. *J. Am. Chem*. Soc. **1989**, *111*, 3860−3869.
(53) Antoni, J.; Grodzicki, M.; Trautwein, A. X.; Bill, E. *J. Phys. Chem. A* **1997**, *101*, 2692−2701.
(54) Ayougou, K.; Mandon, D.; Fischer, J.; Weiss, R.; Müther, M.; Schünemann, V.; Trautwein, A. X.; Bill, E.; Terner, J.; Jayaraj, K.; Gold, A.; Austin, R. N. *Chemistry—Eur. J.* **1996**, *2*, 207−211.
(55) Fujii, H.; Yoshimura, T.; Kamada, H. *Inorg. Chem*. **1996**, *35*, 2373−2377.

C_β interaction in the a_{2u} MO is bonding, so that abstraction of an electron from the a_{2u} MO weakens the $C_\beta-C_\beta$ bond and causes a downshift in these modes.[56] In the case of the iron porphyrin $|Fe^{IV}{=}O\ TMP|^+$, where the porphyrin π-cation radical is considered to be in a nearly pure $^2A_{2u}$ symmetry state, ν_2 of its compound I analogue shifts down in frequency by 40 cm^{-1} relative to the ferric complex.[42,43,57] On the other hand, ν_2 shifts up in frequency by 22 cm^{-1} in the $^2A_{1u}$ compound I analogue generated from iron(III) β-tetramethyl-β-tetramesitylporphyrin.[54,58] Since the symmetry state sensitive markers in the resonance Raman spectra of $|Fe^{IV}{=}O$ **1**$|^+$ and $|Fe^{IV}{=}O$ **2**$|^+$ shift to higher frequency, the singly occupied MOs of the porpholactone π-cation radicals appear to have considerable a_{1u} character, supporting the electronic structure based on ^{1}H NMR, EPR, and Mössbauer data presented in this study.

The crystal structure of $|Fe^{III}$(Cl) **2**$|$ demonstrates that the transformation of one of the pyrrole rings in the porphyrin macrocycle to an oxazolone ring introduces minimal asymmetry in the equatorial bonding of iron. Moreover, the characterization of the Fe═O unit in the compound I analogue by resonance Raman spectroscopy indicates that the structural change in the macrocycle periphery does not perturb the nature of the oxoferryl unit in the high-valent complexes. The similarity of Fe═O frequencies of compound I analogues of meso-substituted porpholactones, porphyrins, and chlorins suggests that equatorial Fe−N bonding is not strongly perturbed by the changes in structure at the molecular periphery. Furthermore, under the experimental conditions described herein, $\nu_{Fe=O}$ for the $^2A_{1u}$ compound I analogues of the chlorin[30] and β-tetramethyl-β-tetramesitylporphyrin,[54,58] as well as the compound I analogues of the porpholactones, are not substantially different from the frequencies observed for the $^2A_{2u}$ porphyrin complexes.[42] This observation suggests that electronic symmetry state may not be a critical determinant of Fe═O stretch in compound I analogues.

The similarity of the Fe═O frequencies of the oxoferryl and oxoferryl porpholactone π-cation radicals is interesting because of the indication that the oxidation level of the porpholactone macrocycle does not to exert an appreciable effect on the Fe═O unit. Such invariance of the Fe═O stretch with the oxidation state of the heme ligand has also been observed for oxoferryl porphyrins and corresponding oxoferryl porphyrin π-cation radicals generated in the presence of the weakly coordinating sixth ligand methanol.[42]

In summary, ferric, oxoferryl, and oxoferryl π-cation radical complexes of novel porpholactone ligands have been characterized. Ligand-centered properties show effects dependent on altered molecular symmetry and peripheral π-conjugation. By contrast, the changes in the peripheral structure of the ligand do not change the characteristics of the oxoferryl unit in the compound I and compound II analogues relative to the corresponding porphyrin species. Further investigation of properties which involve communication between the macrocycle and iron center may shed light on mechanisms by which nature modulates chemistry at metal centers of porphyrin and porphyrin-derived prosthetic groups through changes in ligand substituents, planarity, and symmetry.

Acknowledgment. This work was supported in part by USPHS Grants ES03433 (A.G.) and GM34443 (J.T.), Centre National de la Recherche Scientifique grant UA424 (R.W.), and the Deutsche Forschungsgemeinschaft (A.X.T. and E.B.). A.X.T. and R.W. thank the European HCM network "MASIMO" and the Alexander von Humboldt Foundation for financial support. A.G. and R.W. also thank the NSF for the collaborative grant INT9314422.

IC970597S

(56) Macor, K. A.; Czernuszewicz, R. S.; Spiro T. G. *Inorg. Chem.* **1990**, *29*, 1996−2000.
(57) Czarnecki, K.; Nimri, S.; Gross, Z.; Proniewicz, L. M.; Kincaid, J. R. *J. Am. Chem. Soc.* **1996**, *118*, 2929−2935.
(58) Czarnecki, K.; Proniewicz, L. M.; Fujii, H.; Kincaid, J. R. *J. Am. Chem. Soc.* **1996**, *118*, 4680−4685.